Multi-shell multi-tissue fODF tractography improves V1-V2 macaque connectivity mapping

Guillaume Theaud[1], Maxime Descoteaux[1], Rémi Cossette-Roberge[1], Jean-Christophe Houde[1], Chuyang Ye[2], Nathalie Richard[4], Yujie Hou[3], Loïc Magrou[3], Kenneth Knoblauch[3], Henry Kennedy[3], Bassem Hiba[4]

[1]Sherbrooke Connectivity Imaging Lab (SCIL), University of Sherbrooke
Sherbrooke, QC, Canada

[2]Brainnetome Center, Institute of Automation,
Chinese Academy of Sciences, Beijing, China

[3]Université Claude Bernard Lyon 1,
Inserm, Stem Cell and Brain Research Institute U1208, Bron, France.

[4]Institut des Sciences Cognitives Marc Jeannerod
CNRS/université Lyon1 (UMR 5229), Bron, France.

Synopsis. *We show that multi-shell (multi b-value), multi-directional, and high spatial resolution (300 microns isotropic) diffusion MRI combined with multi-tissue fiber orientation distribution function (fODF) tractography increases by 6% the number of true positive connections and uniformly increases the cortical coverage by 3%, while preserving the same percentage of false positive connections, with respect to a more standard single-tissue single-shell tractography. As a result, it is possible to find all 5 ground truth V1-V2 bundles (true positives), while reconstructing only 4 invalid bundles (false positives) corresponding to 4 pairs of spatially neighboring regions.*

1. Purpose

Validation of global structural connectivity is extremely challenging and the ground truth difficult to obtain. Currently, all validation studies for structural connectivity are based on the use of a single b-value dMRI, also called single-shell, for different high spatial resolutions and a range of number of gradients directions (see Table 1)[1,2,3,4,5,6]. The limitation of single-shell dMRI is that only the white matter tissue fODF is properly modeled through the fODF reconstruction, which leads to known gyral bias near the cortex, free water contamination in regions of partial volume with CSF, and partial voluming with deep nucleii[7,8].

The purpose of this work is twofold: i) To investigate the applicability of multi-shell, multi-directional, and high spatial resolution dMRI for connectivity mapping of V1-V2 of the macaque visual field. ii) To investigate the importance of multi-shell multi-tissue (msmt) fODF reconstruction as opposed to single-tissue fODFs.

2. Dataset

Diffusion-weighted (DW) images were acquired at 7 Tesla (Biospec 70/20, Brucker) with a three shells scheme, b=2000, 4000, 6000 mm^2/s; 64 directions, one b=0 per shell

(Figure 1a), isotropic 300 μm spatial resolution, 4 averages and total imaging time of 38 hours. All DW-images were bias-corrected using N4 and registered on the first b0 image. A three-tissue class segmentation was computed from the first eigenvalue map using the unified segmentation tool of SPM5/8[9] and the Mclaren-rhesus-macaque-atlas a priori maps[10]. The segmentation was manually corrected and cortical V1-V2 ground truth regions labeled by 2 experts (Figure 1c).

3. fODF Reconstruction & Tractography

First, we computed the response functions for the single-[11,12] and multi-tissue[8] spherical deconvolution from the eigenvalue maps computed from the lower shell b2000 dMRI data (Figure 1b), using spherical harmonics of order 8 in Dipy[13]. Next, we used the anatomically constrained Particle Filtering Tractography algorithm[14]. It reduces some of the tractography biases in regions of partial volume and is more robust for quantitative connectivity analysis. We seeded from the GM/WM interface to obtain 1 million streamlines and kept streamlines in the [0.3, 15] mm range. Finally, the connectivity matrix of the number of streamlines (tract-count) connecting each pair of regions was reconstructed with a robust in-house streamline-grid intersection.

3.1. Evaluation

Tract-tracing is considered to be the gold standard for connectivity mapping, due to its precision and repeatability[15,16]. It is now understood that the V1 to V2 connectivity is retinotopic (i.e. the spatial arrangement of retina inputs is respected and can be mapped onto those areas) and point-to-point[17,18], as shown in Figure 1d. There are therefore 5 valid bundles (VB) and a potential for 45 invalid bundles (IB)[19]. We thus computed valid connections (VC) and invalid connections (IC) as in[19], and percentage of cortical coverage.

4. Results

In Figures 2A,B, we see the raw and un-thresholded connectivity matrix and tract-count per pair of regions for multi-tissue fODFs. Overall, we note that msmt fODF tractography produces more valid connections (6.8% increase), while keeping a low increase in invalid connections (0.6% increase). Figure 2B shows 21 reconstructed invalid bundles (4 times the number of valid bundles as similarly reported in[19]). Single-shell single-tissue results (not shown here) are the same as the multi-shell single-tissue results.

Using a threshold at 12000 streamlines (1% of the total number of initial tractography seeds) leads to find all valid bundles and only 4 large invalid bundles, for a total of 65% of valid and 35% of invalid connections.

Finally, multi-shell multi-tissue fODF also shows a 3% improvement in cortical coverage (Table 2). All labels are better covered by the msmt fODF tractography algorithm. From highest to lowest, we note that the central and lower-field parts of the visual field are easier to connect than the upper-field parts.

5. Discussion & Conclusion

Visualizing the 4 densest invalid bundles shows that these connect side-by-side cortical ROIs, where invalid connections are positioned at the boundary of neighbouring labels.

This suggests that the "ground truth" labels and tract-tracing maps may not perfectly reflect the individual macaque's anatomy. A more precise individual-macaque based segmentation, potentially informed by tractography and other imaging modalities, could boost validation results.

In conclusion, we have shown that multi-shell multi-tissue fODF tractography improves connectivity mapping of the V1-V2 macaque connectivity. Further experiments are needed to determine a lower-bound for the number of shells and number of directions best suited for high resolution macaque dMRI tractography technologies. Validation between one invidual macaque histology measurements of labeled neurons and quantitative connectivity measures from in vivo and ex vivo tractography from the same macaque's cortical parcellation is a tremendous open challenge.

References

[1] C. Thomas, F. Q. Ye, M. O. Irfanoglu, P. Modi, K. S. Saleem, D. A. Leopold, C. Pierpaoli, Anatomical accuracy of brain connections derived from diffusion MRI tractography is inherently limited, Proc. Natl. Acad. Sci. 111 (2014) 16574–16579.

[2] E. Calabrese, A. Badea, G. Cofer, Y. Qi, G. A. Johnson, A Diffusion MRI Tractography Connectome of the Mouse Brain and Comparison with Neuronal Tracer Data, Cereb. Cortex 25 (2015) 4628–4637.

[3] H. Azadbakht, L. M. Parkes, H. A. Haroon, M. Augath, N. K. Logothetis, A. de Crespigny, H. E. D'Arceuil, G. J. M. Parker, Validation of High-Resolution Tractography Against In Vivo Tracing in the Macaque Visual Cortex, Cereb. Cortex 25 (2015) 4299–4309.

[4] T. R. Knösche, A. Anwander, M. Liptrot, T. B. Dyrby, Validation of tractography: Comparison with manganese tracing, Hum. Brain Mapp. 36 (2015) 4116–4134.

[5] M. P. van den Heuvel, M. A. de Reus, L. Feldman Barrett, L. H. Scholtens, F. M. Coopmans, R. Schmidt, T. M. Preuss, J. K. Rilling, L. Li, Comparison of diffusion tractography and tract-tracing measures of connectivity strength in rhesus macaque connectome, Hum. Brain Mapp. 36 (2015) 3064–3075.

[6] C. J. Donahue, S. N. Sotiropoulos, S. Jbabdi, M. Hernandez-Fernandez, T. E. Behrens, T. B. Dyrby, T. Coalson, H. Kennedy, K. Knoblauch, D. C. Van Essen, M. F. Glasser, Using Diffusion Tractography to Predict Cortical Connection Strength and Distance: A Quantitative Comparison with Tracers in the Monkey, J. Neurosci. 36 (2016) 6758–6770.

[7] S. Jbabdi, H. Johansen-Berg, Tractography: Where Do We Go from Here?, Brain Connectivity 1 (2011) 169—-183.

[8] B. Jeurissen, J.-D. Tournier, T. Dhollander, A. Connelly, J. Sijbers, Multi-tissue constrained spherical deconvolution for improved analysis of multi-shell diffusion MRI data, Neuroimage 103 (2014) 411–426.

[9] J. Ashburner, K. J. Friston, Unified segmentation, Neuroimage 26 (2005) 839–851.

[10] D. G. McLaren, K. J. Kosmatka, T. R. Oakes, C. D. Kroenke, S. G. Kohama, J. A. Matochik, D. K. Ingram, S. C. Johnson, A population-average MRI-based atlas collection of the rhesus macaque, Neuroimage 45 (2009) 52–59.

[11] M. Descoteaux, R. Deriche, T. R. Knösche, A. Anwander, Deterministic and probabilistic tractography based on complex fibre orientation distributions, IEEE Transactions in Medical Imaging 28 (2009) 269–286.

[12] J. D. Tournier, F. Calamante, A. Connelly, Robust determination of the fibre orientation distribution in diffusion MRI: Non-negativity constrained super-resolved spherical deconvolution, Neuroimage 35 (2007) 1459–1472.

[13] E. Garyfallidis, M. Brett, B. Amirbekian, A. Rokem, S. Van Der Walt, M. Descoteaux, I. Nimmo-Smith, Dipy, a library for the analysis of diffusion mri data, Frontiers in Neuroinformatics 8 (2014).

[14] G. Girard, K. Whittingstall, R. Deriche, M. Descoteaux, Towards quantitative connectivity analysis: Reducing tractography biases, Neuroimage 98 (2014) 266–278.

[15] J. H. Kaas, C. S. Lin, Cortical projections of area 18 in owl monkeys., Vision Res. 17 (1977) 739–41.

[16] M. Wong-Riley, Reciprocal connections between striate and prestriate cortex in squirrel monkey as demonstrated by combined peroxidase histochemistry and autoradiography., Brain Res. 147 (1978) 159–64.

[17] J. Tigges, W. B. Spatz, M. Tigges, Reciprocal point-to-point connections between parastriate and striate cortex in the squirrel monkey (Saimiri), J. Comp. Neurol. 148 (1973) 481–489.

[18] J. Tigges, W. B. Spatz, M. Tigges, Efferent cortico-cortical fiber connections of area 18 in the squirrel monkey (Saimiri), J. Comp. Neurol. 158 (1974) 219–235.

[19] K. H. Maier-Hein, P. Neher, J. Christophe, M.-A. Cote, E. Garyfallidis, J. Zhong, M. Chamberland, F.-C. Yeh, Y. C. Lin, Q. Ji, W. E. Reddick, J. O. Glass, D. Q. Chen, Y. Feng, C. Gao, Y. Wu, J. Ma, H. Renjie, Q. Li, C.-F. Westin, S. Deslauriers-Gauthier, J. O. O. Gonzalez, M. Paquette, S. St-Jean, G. Girard, F. Rheault, J. Sidhu, C. M. W. Tax, F. Guo, H. Y. Mesri, S. David, M. Froeling, A. M. Heemskerk, A. Leemans, A. Bore, B. Pinsard, C. Bedetti, M. Desrosiers, S. Brambati, J. Doyon, A. Sarica, R. Vasta, A. Cerasa, A. Quattrone, J. Yeatman, A. R. Khan, W. Hodges, S. Alexander, D. Romascano, M. Barakovic, A. Auria, O. Esteban, A. Lemkaddem, J.-P. Thiran, H. E. Cetingul, B. L. Odry, B. Mailhe, M. Nadar, F. Pizzagalli, G. Prasad, J. Villalon-Reina, J. Galvis, P. Thompson, F. Requejo, P. Laguna, L. Lacerda, R. Barrett, F. Dell'Acqua, M. Catani, L. Petit, E. Caruyer, A. Daducci, T. Dyrby, T. Holland-Letz, C. Hilgetag, B. Stieltjes, M. Descoteaux, The challenge of mapping the human connectome based on diffusion tractography, Nature communications in press (2017).

[20] T. Dhollander, R. E. Smith, J.-D. Tournier, B. Jeurissen, A. Connelly, Time to move on: an FOD-based DEC map to replace DTI's trademark DEC FA, Proc. Intl. Soc. Mag. Reson. Med (2015) 1027.

Study	Image resolution	Field Strength	b-values (in mm^2/s)	Number of directions
Thomas et al 2014 (macaque)	0.25mm	7.0T	4800	121
Calabrese et al 2015 (mouse)	0.042mm	9.4T	4000	120
Azadbakht et al 2015 (macaque)	0.8mm 0.43mm	4.7T	4000 8000	61 120
Knosche et al 2015 (pig)	0.51mm	4.7T	4009	61
Van den Heuvel et al 2015 (macaque)	1,1mm	3T	1000	60
Donahue et al 2016 (macaque)	0.43mm	4.7T	4000 8000	61 120
present study (macaque)	0.3mm	7.0T	2000,4000,6000	64,64,64

Table 1. Review of dMRI acquisition in previous connectivity validation studies

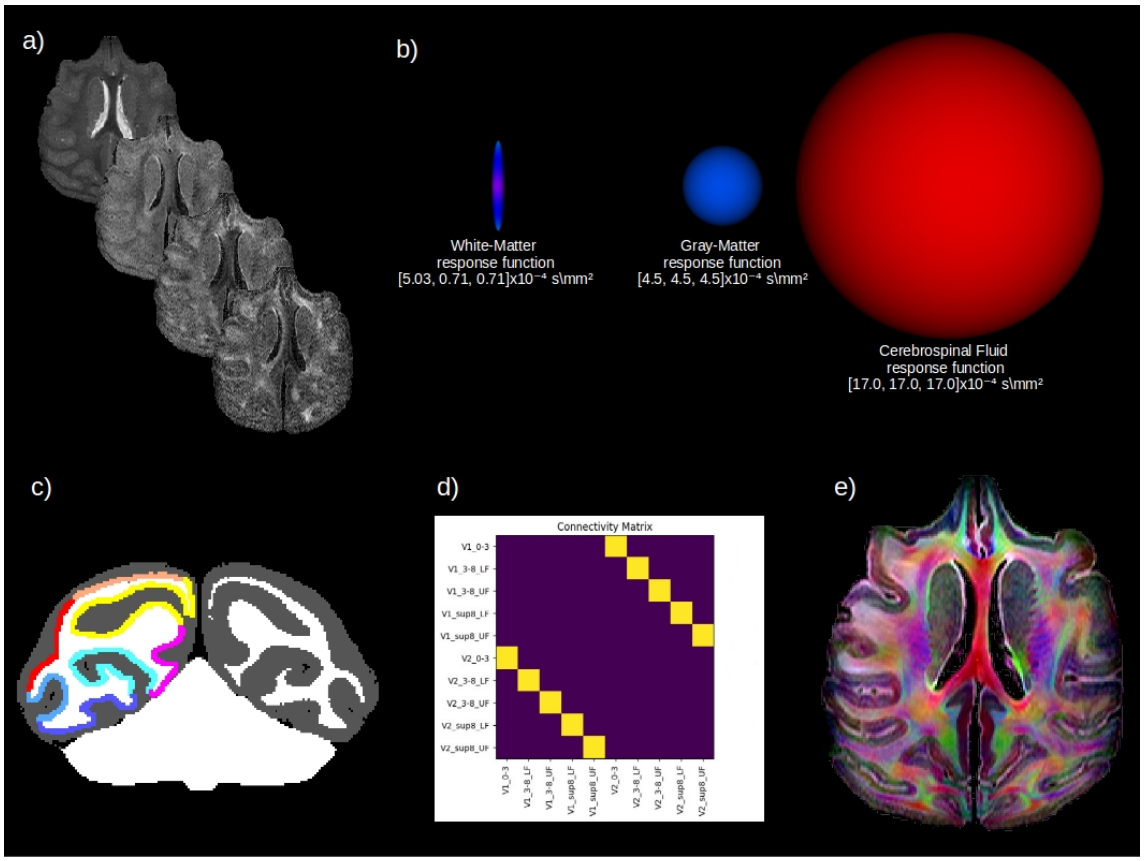

Figure 1. In a), we see the b=0,2000,4000,6000 mm^2/s, b) the WM/GM/CSF response functions used to compute the fODFs, c) the labels overlaid on the WM (white) and GM (gray) tissue maps, in d) the ground truth V1-V2 connectivity matrix (0-3: central, 3-8: paracentral, sup8: far periphery, LF: lower-field, UF: upper-field), and e) the multi-tissue fODF RGB image[20].

.

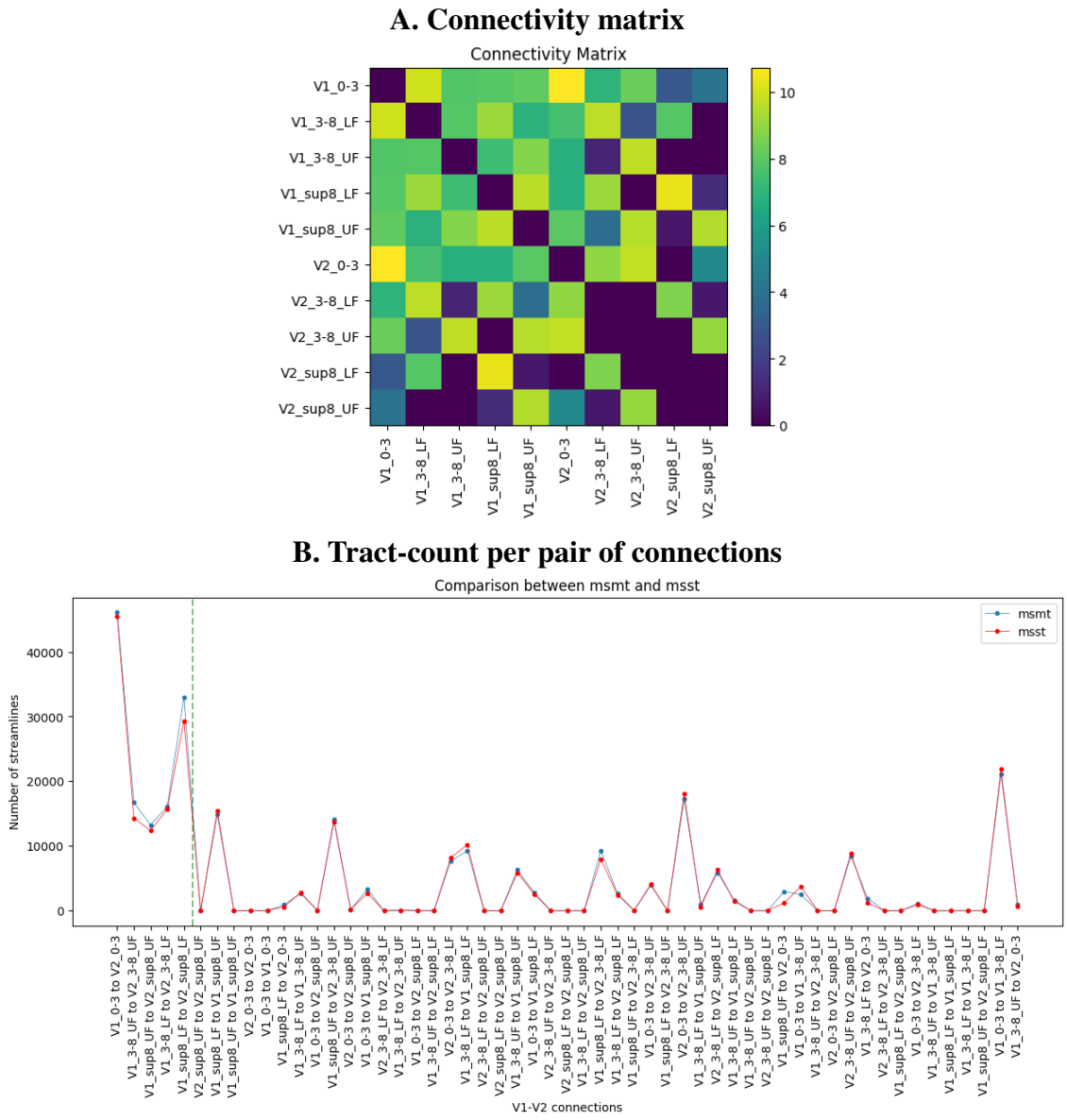

Figure 2. The results with the raw and un-thresholded data. In A, the connectivity matrix. In B, the tract-count per pair of connections. To the left of the dashed green line, we have the 5 valid bundles and to the right, the invalid bundles. Single-shell single-tissue results (not shown here) are the same as the multi-shell single-tissue results.

A. Connectivity matrix

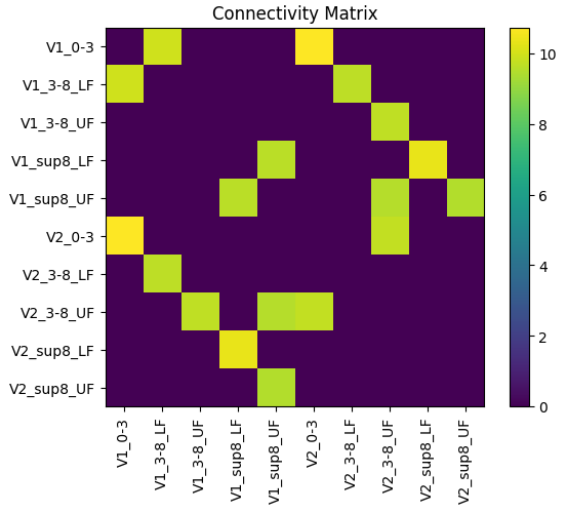

B. Tract-count per pair of connections

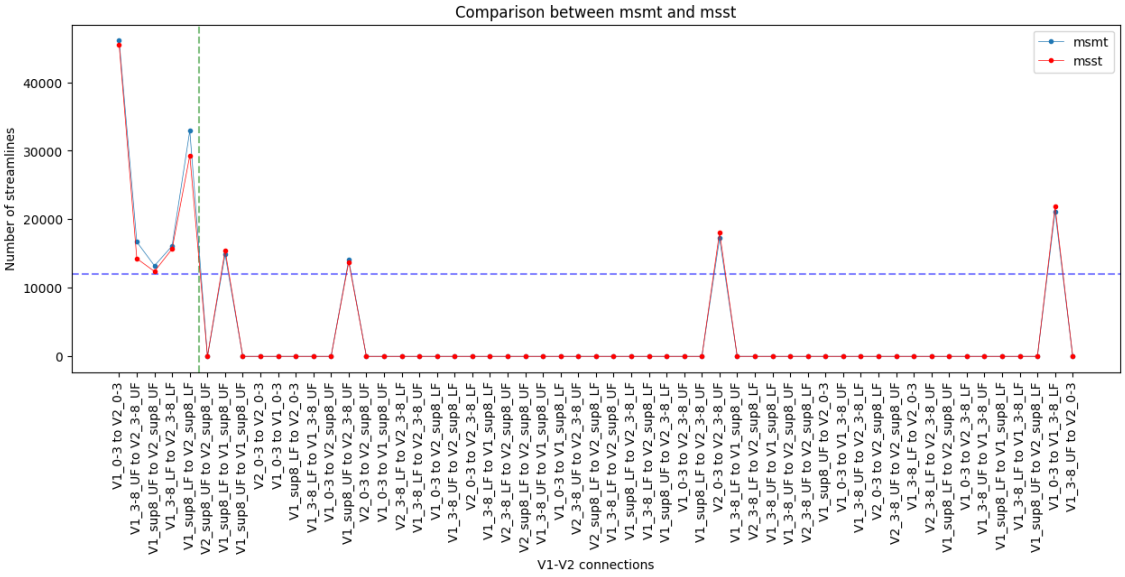

Figure 3. The results with a threshold at 12000 streamlines. In A, the connectivity matrix. In B, the tract-count per pair of connections. Single-shell single-tissue results (not shown here) are the same as the multi-shell single-tissue results.

Percentage of coverage for the single tissue vs multi tissue fODF tractography

Connection	Total percentage	Percentage per label
V1_0-3/V2_0-3	57% / 58%	V1_0-3: 64% / 66% V2_0-3: 52% / 52%
V1_3-8_LF/V2_3-8_LF	52% / 53%	V1_3-8_LF: 44% / 44% V2_3-8_LF: 63% / 65%
V1_3-8_UF/V2_3-8_UF	27% / 29%	V1_3-8_UF: 37% / 39% V2_3-8_UF: 24% / 25%
V1_sup8_LF/V2_sup8_LF	45% / 49%	V1_sup8_LF: 37% / 40% V2_sup8_LF: 59% / 63%
V1_sup8_UF/V2_sup8_UF	33% / 36%	V1_sup8_UF: 26% / 28% V2_sup8_UF: 51% / 56%

Table 2. Percentages of coverage for each true connection (single-tissue vs multi-tissue).